Research Article GU J Sci 37(4): 1770-1789 (2024) DOI: 10.35378/gujs.1374222

Gazi University

Journal of Science

http://dergipark.gov.tr/gujs

Iterative Root-Finding Algorithm for Accurate Parameter Extraction of Solar Photovoltaic Cells

Moulay Rachid DOUIRI *

Department of Applied Physics, Faculty of Science and Technology, Cadi Ayyad University, Marrakesh, 40 000, Morocco

Highlights

- Enhanced IRF algorithm precisely extracts parameters from the single diode model.
- This novel method's effectiveness is demonstrated on three different PV modules.
- A comparative analysis is conducted with modern algorithms.
- The method proves effective under varying sun irradiance and temperature conditions.

Article Info

Received:11 Oct 2023
Accepted: 24 June 2024

Keywords

Parameters extraction
Root-finding algorithm
Single diode model
Solar cells

Abstract

The performance of photovoltaic models depends significantly on the accuracy of their parameters, which are determined by the chosen method and objective function. Extracting these parameters accurately under different environmental conditions is essential to enhance reliability, accuracy, and minimize system costs. In this research, a novel technique is proposed for extracting the electrical parameters of the solar cell single diode model, including saturation current, serial resistance, parallel resistance, and ideality factor. To overcome the challenges posed by the chaotic behavior of the *I-V* curve equation, an improved Iterative Root-Finding algorithm is introduced. This algorithm acts as an optimization tool, increasing the likelihood of obtaining highly accurate solutions by minimizing the quadratic error between experimental and theoretical characteristics in a shorter time frame. The numerical and experimental results demonstrate the effectiveness of this approach in solar module modeling, showing squared errors approaching zero. This study opens new possibilities for improving the accuracy and reliability of photovoltaic models, leading to more efficient solar energy systems.

1. INTRODUCTION

In recent years, photovoltaic (PV) systems have emerged as one of the most promising and sustainable solutions to meet the ever-growing global demand for renewable energy. These systems harness the power of sunlight to convert it into clean electricity, presenting an environmentally friendly alternative to conventional energy sources [1]. To optimize the performance and efficiency of PV systems, accurate parameter extraction is paramount. The precise determination of parameters, such as series and shunt resistances, ideality factor, and saturation current, is crucial for the accurate modeling and characterization of PV devices [2]. However, accurate parameter extraction in PV systems remains a challenging task due to various factors, such as temperature variations, manufacturing defects, and real-world operating conditions [3]. Traditional parameter extraction techniques often encounter difficulties in providing reliable results, especially when dealing with non-linear behaviors and complex electrical characteristics of PV devices [3].

PV generators are mostly nonlinear systems, and their behavior strongly depends on environmental conditions. Consequently, the variations in illumination and temperature during the daytime affect the current-voltage (*I-V*) and power-voltage (*P-V*) characteristics of the PV modules [3]. The *I-V* curve of a solar cell shows a nonlinear characteristic determined by the parameters of the solar cell describing its shape. To better understand the behavior of a solar cell, an equivalent circuit model with grouped

* e-mail: douirirachid@hotmail.com

parameters is often used to simulate its performance under different conditions. Two models are commonly used for the PV electrical modeling: the single diode model and the double diode model [4]. The single diode model contains five components represented by five adjustable parameters: photocurrent I_{ph}, saturation current I_{sat}, diode ideality factor n, series resistance R_s (which illustrates the *ohmic* loss due to the large amount of resistive semiconductor material and metallic contacts), and the shunt resistance R_{sh} (which explains the leakage current in the *p-n* junction). The double diode model contains an additional diode, which adds a second saturation current I_{sat2} and a diode ideality factor n_2 [5]. Previously reported works have mostly used the single diode model, assuming that the recombination loss is negligible in the space charge region, which is responsible for calculating the second diode in the equivalent circuit of the solar cell [6].

Over the years, several approaches have been developed to extract solar cell parameters. Three main approach groups were presented: The first ones are the analytical methods, which are characterized by their simplicity and their speed of calculation. However, they often lack precision as they are based on a number of assumptions. Moreover, since the parameters are deduced on the basis of a few selected points, the solutions are more sensitive to measurement noise [7]. One can quote some works like the method of analysis in five points and the method of the least squares of nonlinear error [8]. The second approach is the deterministic methods, which are often gradient-based. Despite their effectiveness in local researches, they hesitate on a number of limitations: these approaches are very sensitive to initial values and are demanding in terms of differentiability and convexity, like *Newton's* approach [9] and the nonlinear algorithm method [10]. Furthermore, in reference [11], an innovative enhancement to *Newton's* method is proposed. This improvement involves the integration of the Two-Point Bracketing method and the Inverse Quadratic Interpolation method, leading to high-order convergence and remarkable efficiency.

Other researchers have conducted investigations into various metaheuristic algorithms to achieve precise and dependable results. The Dandelion Optimization Algorithm (DOA) is introduced in [12] for precise extraction of solar PV panel parameters, exhibiting versatility across different module types. The study rigorously tests DOA on single-diode and double-diode PV models, including *monocrystalline*, *polycrystalline*, and *thin-film* technologies. Notably, the research provides a thorough evaluation by conducting comprehensive statistical analyses and comparing DOA with two existing hybrid optimization algorithms from the literature. In Reference [13], the utilization of Snake optimization metaheuristic algorithms is proposed, and an enhanced version demonstrates promising outcomes compared to several other algorithms. Another algorithm, the Elite Learning Adaptive Differential Evolution (ELADE), introduced in Reference [14], combines strategies to strike a balance between avoiding local optima and accelerating convergence. Similarly, Reference [15] introduces the Memory-based Improved Gorilla Troops Optimizer (MIGTO), which outperforms other algorithms in extracting parameters for photovoltaic models. In the pursuit of improved Maximum Power Point Tracking (MPPT) applications, Reference [16] proposes a modified Normative Fish Swarm Algorithm (mNFSA), which surpasses other optimization algorithms. Additionally, Reference [17] presents a parameter identification method based on radial basis functions (RBF), significantly enhancing the accuracy of PV cell modeling. Lastly, Reference [18] employs the Artificial Hummingbird Optimization (AHO) algorithm for parameter extraction, achieving competitive results compared to other state-of-the-art algorithms.

While numerous studies have explored parameter estimation in PV models, our research stands out due to its unique focus on the construction of the objective function. Unlike prior works, we delve into the methodologies for solving the equations of nonlinear, multi-variable, and complex PV models using both datasheet information and actual experimental data. Notably, no review papers have explored this specific aspect of PV modeling. Our contribution lies in the development of the Iterative Root-Finding Algorithm (IRF), a novel approach designed for efficiently determining unknown parameters within the single diode PV model. The IRF, characterized by guaranteed convergence, addresses a critical gap in the literature by offering a robust solution to the optimization problem. Crucially, we utilize actual measured laboratory data collected under diverse environmental conditions, setting our study apart from simulations or theoretical models commonly found in the literature. The application of the IRF to real-world data demonstrates its superior performance across various statistical criteria and environmental scenarios. Comparative analysis

with existing approaches in the literature reveals that the IRF outperforms in terms of accuracy, stability, and convergence rate, all while maintaining a reasonable processing time. This demonstrates the practical significance and efficiency of our proposed algorithm.

This paper is divided into three main sections: the first section focuses on the modeling of the solar cell single diode, the second section delves into the extraction of electrical parameters using the enhanced IRF algorithm, and the third section provides the analysis where the authors present, interpret, and compare the simulated and experimental results they obtained with algorithms proposed by other researchers in the existing literature.

2. SOLAR CELL SINGLE DIODE MODEL

The equivalent circuit of a solar cell, shown in Figure 1, is represented by a *p-n* junction diode, a current source I_{ph}, a series resistance R_s, and a shunt resistance R_{sh} (a full list of notations follows the "Conclusion" section). The R_s represents the loss due to the Joule effect caused by series resistances due to the resistivity of the semiconductor material, the contact resistance, the resistance of the collector gate, and the current collected by the bus [19]. The normal value of this resistance is very low, tens of *ohms*, which directly reflects the quality of the manufactured PV cells [20]. Additionally, the R_{sh} indicates the internal loss or the leakage current through the *Shockley* diode [20]. In other words, R_{sh} represents the leakage conductivity. Furthermore, the current proportional to the voltage is developed in addition to the diode current, acting as if the photo-current needs to be reduced. To find the relationship between the output current I_{pv} and the output voltage V_{pv}, *Kirchhoff's* law is used on the below equivalent circuit (Figure 1) [21]:

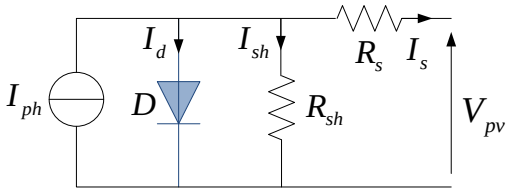

Figure 1. *Single diode model's circuit equivalence for solar cells*

The relationship between the current and the voltage can be written as follows:

$$I_{pv} = I_{ph} - I_d - I_{sh}\,. \tag{1}$$

I_d is proportional to the saturation current, and it can be written as follows [22]:

$$I_d = I_0\left(\exp\left(\frac{q\left(V_{pv} + R_s I_{pv}\right)}{TKnN_c}\right) - 1\right). \tag{2}$$

I_{sh} can be written as follows:

$$I_{sh} = \frac{V_{pv} + R_s I_{pv}}{R_{sh}}\,. \tag{3}$$

By substituting in Equation (1), the characteristic current-voltage equation of a PV cell can be written as follows:

$$I_{pv} = I_{ph} - I_0\left(\exp\left(\frac{q\left(V_{pv} + R_s I_{pv}\right)}{TKnN_c}\right) - 1\right) - \frac{V_{pv} + R_s I_{pv}}{R_{sh}}\,. \tag{4}$$

The photo-current mainly depends on the illumination and the temperature of a functional solar cell and can be given as follows [23]:

$$I_{ph} = \frac{G}{G_{rf}}\left(I_{sc} + k_i\left(T - T_{rf}\right)\right). \tag{5}$$

The saturation current I_0 can be written as follows:

$$I_0 = I_{rs}\left(\frac{T}{T_{rf}}\right)^3 \exp\left(\frac{qE_g\left(\frac{1}{T_{rf}} - \frac{1}{T}\right)}{Kn}\right). \tag{6}$$

The saturation current changes with temperature of the solar cell, and can be written as follows (7):

$$I_{rs} = \frac{I_{sc}}{\exp\left(\frac{qV_{oc}}{TKnN_c}\right) - 1}. \tag{7}$$

The five characteristic parameters of this model are: I_{ph}, I_0, R_s, R_{sh} and n.

3. IMPROVED ITERATIVE ROOT-FINDING ALGORITHM

The current-voltage relationship of a PV cell is given by the following equation:

$$I_{pv} = I_{ph} - I_0\left(\exp\left(\frac{V_{pv} + R_s I_{pv}}{V_t}\right) - 1\right) - \frac{V_{pv} + R_s I_{pv}}{R_{sh}} \tag{8}$$

with the thermal voltage of the diode is given by the following equation:

$$V_t = \frac{TKnN_c}{q}. \tag{9}$$

Equation (8) can be transformed into the form of Equation (10) when considering the *I-V* relationship under reference conditions.

$$I_{pv} = I_{phrf} - I_{0rf}\left(\exp\left(\frac{V_{pv} + R_{srf} I_{pv}}{V_{trf}}\right) - 1\right) - \frac{V_{pv} + R_{srf} I_{pv}}{R_{shrf}} \tag{10}$$

where I_{phrf}, I_{0rf} ,n_{rf}, R_{srf}, R_{shrf} are evaluated at a particular point on the *I-V* characteristics curve.

The derivation and solution of Equations (18), (19), (22), (29), and (30) serve as crucial steps to determine the five unknown parameters (I_{ph}, I_0, n, R_s, and R_{sh}) accurately. These equations are derived from the fundamental current-voltage relationship (Equation 10) under different conditions (such as short circuit, open circuit, and maximum power point) and are necessary to express the model parameters in terms of measurable quantities. By solving these intermediate equations, we establish a consistent and reliable framework to compute the parameters needed for the main set (Equations (32) – (36)). This ensures that the iterative root-finding algorithm can effectively minimize the error term and accurately model the PV cell characteristics.

At the point of short circuit: $I_{pv}=I_{sc}$, $V_{pv}=0$.

$$I_{scrf} = I_{phrf} - I_{0rf}\left(\exp\left(\frac{R_{srf} I_{scrf}}{V_{trf}}\right) - 1\right) - \frac{R_{srf} I_{scrf}}{R_{shrf}}. \tag{11}$$

At the open circuit point: $I_{pv}=0$, $V_{pv}=V_{oc}$,

$$I_{phrf} - I_{0rf}\left(\exp\left(\frac{V_{ocrf}}{V_{trf}}\right)-1\right)-\frac{V_{ocrf}}{R_{shrf}}=0. \tag{12}$$

At MPP : $I_{pv}=I_m$, $V_{pv}=V_m$, we can write:

$$I_{mrf} = I_{phrf} - I_{0rf}\left(\exp\left(\frac{V_{mrf}+R_{srf}I_{mrf}}{V_{trf}}\right)-1\right)-\frac{V_{mrf}+R_{srf}I_{mrf}}{R_{shrf}}. \tag{13}$$

In equation (10), at the open-circuit voltage under STC, the derivative of current with respect to voltage is equal to the R_{srf}. The exact expressions for the derivatives of current with respect to voltage would involve additional terms due to the dependence of the right-hand side of Equation (10) on both V_{pv} and I_{pv}, similar to the form presented in Equation (27). The simplified forms of Equations (14) and (15) are derived under specific conditions that are often encountered in practical applications. Specifically, under open-circuit conditions where $I_{pv}=0$ and $V_{pv}=V_{oc}$, the approximation simplifies because the effect of R_s is minimal. Thus, the derivative dI_{pv}/dV_{pv} predominantly reflects the inverse of R_{sh}, giving rise to Equation (15). Conversely, under short-circuit conditions where $V_{pv}=0$ and $I_{pv}=I_{sc}$, the voltage drop across the series resistance R_s is significant, and the derivative dI_{pv}/dV_{pv} is dominated by the series resistance itself, leading to Equation (14). These approximations hold well under STC typically used in PV performance assessments. However, they may not capture all the nuances of the PV cell behavior under all possible operating conditions. For more precise modeling, the full dependence on V_{pv} and I_{pv} as given by the exact form should be considered

$$\frac{dI_{pv}}{dV_{pv}}=-\frac{1}{R_{srf}}. \tag{14}$$

The differentiation of current with respect to voltage at short-circuit current is equivalent a shunt resistance R_{shrf} in STC:

$$\frac{dI_{pv}}{dV_{pv}}=-\frac{1}{R_{shrf}}. \tag{15}$$

At any point, the reference power of the PV can be written as:

$$P_{pv}=V_{pv}I_{pv}=V_{pv}\left(I_{phrf}-I_{0rf}\left(\exp\left(\frac{V_{pv}+R_{srf}I_{pv}}{V_{trf}}\right)-1\right)-\frac{V_{pv}+R_{srf}I_{pv}}{R_{shrf}}\right). \tag{16}$$

The below parameters are usually given on datasheet information. At MPP, the differentiation of power with respect to voltage is equal to zero, and can be written as follow:

$$\frac{dP_{pv}}{dV_{pv}}=0. \tag{17}$$

In our analysis of photovoltaic cell behavior, we employ several key Equations (18), (19), (22), (29), and (30) to model its dynamic response under varying conditions. It's important to note that these equations are derived under specific assumptions and approximations, which simplify the complex nature of the PV cell's behavior. While not exact, these equations are crucial for deriving comprehensive model Equations (32) - (36) that describe the cell's performance. The approximations made, such as assuming linearity in certain parameters and neglecting higher-order effects under specific conditions, facilitate both the derivation

process and computational feasibility of the model. Despite potential inaccuracies, the inclusion of these approximations is justified by their practical utility in providing reasonable predictions within the scope of our analysis. Transparency regarding these assumptions allows for critical evaluation of their impact on model accuracy and the validity of our findings.

From Equation (12), the generated photo-current I_{phrf} can be obtained as follow:

$$I_{phrf} = I_{0rf}\left(\exp\left(\frac{V_{ocrf}}{V_{trf}}\right)-1\right)+\frac{V_{ocrf}}{R_{shrf}}\,. \tag{18}$$

By substitution the Equation (18) in (11) gives us:

$$I_{scrf} = I_{0rf}\left(\exp\left(\frac{V_{ocrf}}{V_{trf}}\right)-\exp\left(\frac{R_{srf}I_{scrf}}{V_{trf}}\right)\right)+\frac{V_{ocrf}-R_{srf}I_{scrf}}{R_{shrf}}\,. \tag{19}$$

By simplifying the Equation (19), we obtain the Equation (20):

$$I_{scrf} = I_{0rf}\left(\exp\left(\frac{V_{ocrf}}{V_{trf}}\right)\right)+\frac{V_{ocrf}-R_{srf}I_{scrf}}{R_{shrf}}\,. \tag{20}$$

The simplification occurs because the second exponential term, $\exp\left(\frac{R_{srf}I_{scrf}}{V_{trf}}\right)$, is approximately 1 when $R_{srf}I_{scrf} \ll V_{trf}$. This approximation is valid under typical operating conditions of a solar cell where R_{srf} (series resistance) and I_{scrf} (short-circuit current under reference conditions) are such that their product is much smaller compared to V_{trf} (thermal voltage of the diode). Physically, this approximation means that the impact of the second exponential term on I_{scrf} is negligible or very small, allowing us to drop it without significant loss of accuracy in practical calculations. This is justified by the fact that $R_{srf}I_{scrf}$ is typically much smaller compared to V_{trf} in operational scenarios of photovoltaic cells, making the second exponential term inessential for accurate estimation of I_{scrf}. Thus, Equation (19) simplifies to (20).

By solving this equation for I_{0rf}, the Equation (21) is obtained:

$$I_{0rf} = \left(I_{scrf}-\frac{V_{ocrf}-R_{srf}I_{scrf}}{R_{shrf}}\right)\exp\left(-\frac{V_{ocrf}}{V_{trf}}\right). \tag{21}$$

Replacing Equations (21) and (18) with (13) yields Equation (22)

$$I_{mrf} = I_{0rf}-\frac{V_{mrf}+R_{srf}I_{mrf}-R_{srf}I_{scrf}}{R_{shrf}}-\left(I_{0rf}-\frac{V_{0crf}-R_{srf}I_{scrf}}{R_{shrf}}\right)\left(\exp\left(\frac{V_{mrf}+R_{srf}I_{mrf}}{V_{trf}}\right)\right). \tag{22}$$

The Equation (17) can be rewritten as follow:

$$\frac{dP_{pv}}{dV_{pv}} = I_{mrf}+V_{mrf}.\frac{dI_{pv}}{dV_{pv}} = 0\,. \tag{23}$$

This, leads to the Equation (24):

$$\frac{dI_{pv}}{dV_{pv}} = -\frac{I_{mrf}}{V_{mrf}}. \tag{24}$$

Equation (10) is a transcendental equation, which requires some methods to express the current and voltage. Therefore, it is rewritten as Equation (25):

$$I_{pv} = f(I_{pv}, V_{pv}). \tag{25}$$

By differentiating the Equation (25), the following equation can be obtained:

$$dI_{pv} = df(I_{pv}, V_{pv}) = dI_{pv}\frac{\partial f(I_{pv}, V_{pv})}{\partial I_{pv}} + dV_{pv}\frac{\partial f(I_{pv}, V_{pv})}{\partial V_{pv}} \tag{26}$$

so

$$\frac{dI_{pv}}{dV_{pv}} = \frac{\dfrac{\partial f(I_{pv}, V_{pv})}{\partial V_{pv}}}{1 - \dfrac{\partial f(I_{pv}, V_{pv})}{\partial I_{pv}}}. \tag{27}$$

Using Equations (27) and (23), the Equation (27) can be found [24]:

$$\frac{dP_{pv}}{dV_{pv}} = \frac{d(V_{pv}I_{pv})}{dV_{pv}} = I_{mrf} + V_{mrf}\frac{\dfrac{\partial f(I_{pv}, V_{pv})}{\partial V_{pv}}}{1 - \dfrac{\partial f(I_{pv}, V_{pv})}{\partial I_{pv}}} \tag{28}$$

where

$$\frac{dP_{pv}}{dV_{pv}} = I_{mrf} + V_{mrf}\left(\frac{-\left(I_{0rf} - \dfrac{V_{ocrf} - I_{scrf}R_{srf}}{R_{shrf}}\right)\exp\left(\dfrac{V_{mrf} + I_{mrf}R_{srf}}{V_{trf}}\right)}{V_{trf}R_{srf}} - \frac{1}{R_{shrf}}}{1 + \dfrac{\left(I_{0rf} - \dfrac{V_{ocrf} - I_{scrf}R_{srf}}{R_{shrf}}\right)\exp\left(\dfrac{V_{mrf} + I_{mrf}R_{srf}}{V_{trf}}\right)}{V_{trf}R_{shrf}} - \frac{R_{srf}}{R_{shrf}}}\right) = 0. \tag{29}$$

The two Equations (29) and (22) are written with four unknowns, which are R_{srf}, R_{shrf}, I_{0rf} and n_{rf}. The Equations (15), (28) and (29) lead to:

$$-\frac{1}{R_{shrf}} = \frac{\dfrac{-\left(I_{0rf} - \dfrac{V_{ocrf} - I_{scrf}R_{srf}}{R_{shrf}}\right)\exp\left(\dfrac{V_{mrf} + I_{mrf}R_{srf}}{V_{trf}}\right)}{V_{trf}R_{shrf}} - \frac{1}{R_{shrf}}}{1 + \dfrac{\left(I_{0rf} - \dfrac{V_{ocrf} - I_{scrf}R_{srf}}{R_{shrf}}\right)\exp\left(\dfrac{V_{mrf} + I_{mrf}R_{srf}}{V_{trf}}\right)}{V_{trf}R_{shrf}} - \frac{R_{srf}}{R_{shrf}}}. \tag{30}$$

Using Equations (18), (20), (22), (29) and (30), it is possible now to determine the five unknown parameters which are I_{ph}, I_0, n, R_s and R_{sh}. The least square method can be employed to minimize the error term. The value of the error (ε) is computed by summing the squares of the error as following:

$$\varepsilon = \sum_{i=1}^{k}\left(I_i - I_{ph} + I_0\left(\exp\left(\frac{V_i + I_i R_s}{nV_t} \right) - 1 \right) + \frac{V_i + I_i R_s}{R_{sh}} \right)^2 . \tag{31}$$

By conducting partial differentiation with respect to I_{ph}, I_0, n, R_s and R_{sh} and setting them to zero, we obtain the subsequent expressions

$$g_1 = \frac{\partial \varepsilon}{\partial I_{ph}} = -2\sum_{i=1}^{k}\left(I_i - I_{ph} + I_0\left(\exp\left(\frac{V_i + I_i R_s}{nV_t} \right) - 1 \right) + \frac{V_i + I_i R_s}{R_{sh}} \right) = 0 , \tag{32}$$

$$g_2 = \frac{\partial \varepsilon}{\partial I_0} = 2\sum_{i=1}^{k}\left(\exp\left(\frac{V_i + I_i R_s}{nV_t} \right) - 1 \right)\left(I_i - I_{ph} + I_0\left(\exp\left(\frac{V_i + I_i R_s}{nV_t} \right) - 1 \right) + \frac{V_i + I_i R_s}{R_{sh}} \right) = 0 , \tag{33}$$

$$g_3 = \frac{\partial \varepsilon}{\partial n} = -2\sum_{i=1}^{k}\left(\frac{I_0\left(V_i + I_i R_s\right)}{n^2 V_t} \exp\left(\frac{V_i + I_i R_s}{nV_t} \right) \right)\left(I_i - I_{ph} + I_0\left(\exp\left(\frac{V_i + I_i R_s}{nV_t} \right) - 1 \right) + \frac{V_i + I_i R_s}{R_{sh}} \right) = 0 , \tag{34}$$

$$g_4 : \frac{\partial \varepsilon}{\partial R_s} = 2\sum_{i=1}^{k}\left(\frac{I_0 I_i}{nV_T} \exp\left(\frac{V_i + I_i R_s}{nV_t} \right) + \frac{I_i}{R_{sh}} \right)\left(I_i - I_{ph} + I_0\left(\exp\left(\frac{V_i + I_i R_s}{nV_t} \right) - 1 \right) + \frac{V_i + I_i R_s}{R_{sh}} \right) = 0 , \tag{35}$$

$$g_5 : \frac{\partial \varepsilon}{\partial R_{sh}} = -2\sum_{i=1}^{k}\left(\frac{V_i + I_i R_s}{R_{sh}^2} \right)\left(I_i - I_{ph} + I_0\left(\exp\left(\frac{V_i + I_i R_s}{nV_t} \right) - 1 \right) + \frac{V_i + I_i R_s}{R_{sh}} \right) = 0 . \tag{36}$$

The Equations (32), (33), (34), (35) and (36) constitute a set of five non-linear equations with five unknowns, making them solvable. However, due to the implicit nature of these equations, a numerical method must be employed. Therefore, the IRF algorithm is chosen for its rapid convergence and reliable performance. The general form of the IRF algorithm can be expressed as follows:

$$S^{t+1} = S^t - \left(J(S^t) \right)^{-1} \left(g(S)^t \right) \tag{37}$$

with

$$S^{t+1} = \begin{pmatrix} I_{ph}^{t+1} \\ I_0^{t+1} \\ R_{sh}^{t+1} \\ R_s^{t+1} \\ n^{t+1} \end{pmatrix} \tag{38}$$

$$S^t = \begin{pmatrix} I_{ph}^{t} \\ I_0^{t} \\ R_{sh}^{t} \\ R_s^{t} \\ n^{t} \end{pmatrix} \tag{39}$$

$$\left(J(S^t) \right)^{-1} = \begin{pmatrix} a_1 & b_1 & c_1 & d_1 & e_1 \\ a_2 & b_2 & c_2 & d_2 & e_2 \\ a_3 & b_3 & c_3 & d_3 & e_3 \\ a_4 & b_4 & c_4 & d_4 & e_4 \\ a_5 & b_5 & c_5 & d_5 & e_5 \end{pmatrix}^{-1} \tag{40}$$

$$\left(g(S)^t\right)=\begin{pmatrix} g_1\left(I_{ph}^t, I_0^t, R_{sh}^t, R_s^t, n^t\right) \\ g_2\left(I_{ph}^t, I_0^t, R_{sh}^t, R_s^t, n^t\right) \\ g_3\left(I_{ph}^t, I_0^t, R_{sh}^t, R_s^t, n^t\right) \\ g_4\left(I_{ph}^t, I_0^t, R_{sh}^t, R_s^t, n^t\right) \\ g_5\left(I_{ph}^t, I_0^t, R_{sh}^t, R_s^t, n^t\right) \end{pmatrix}. \tag{41}$$

The iteration number is denoted by t. S^{t+1} and S^t are vectors consisting of 5 elements each, representing the succeeding and present values of the 5 parameters, respectively. $J(S^t)$ denotes the *Jacobian* matrix encompassing the partial derivatives of each equation concerning every parameter. Consequently, it is a *5x5* matrix computed based on the current parameter values. $g(S^t)$ denotes the collection of 5 partial derivatives that need assessment for the present parameter values.

To achieve an optimal solution and locate the global minimum, the clear representation of the single diode model, as expressed in Equation (8), is utilized by substituting the calculated 5 parameters at each iteration. This allows for the construction of an *I-V* curve, which is then compared with the measured curve using the mean absolute percentage error (MAPE)

$$MAPE=\frac{100\%}{r}\sum_{i=1}^{r}\left|1-\frac{\tilde{y}_i}{y_i}\right|. \tag{42}$$

In this context, y_i represents the values of I_{ph}, I_0, R_{sh}, R_s, and n obtained directly from the experimental curve, while $\tilde{y}_i$ denotes the same electrical parameter extracted through the *I-V* curve using the single diode model. The five parameters needed for this extraction are estimated separately using explicit and fitting methods for each.

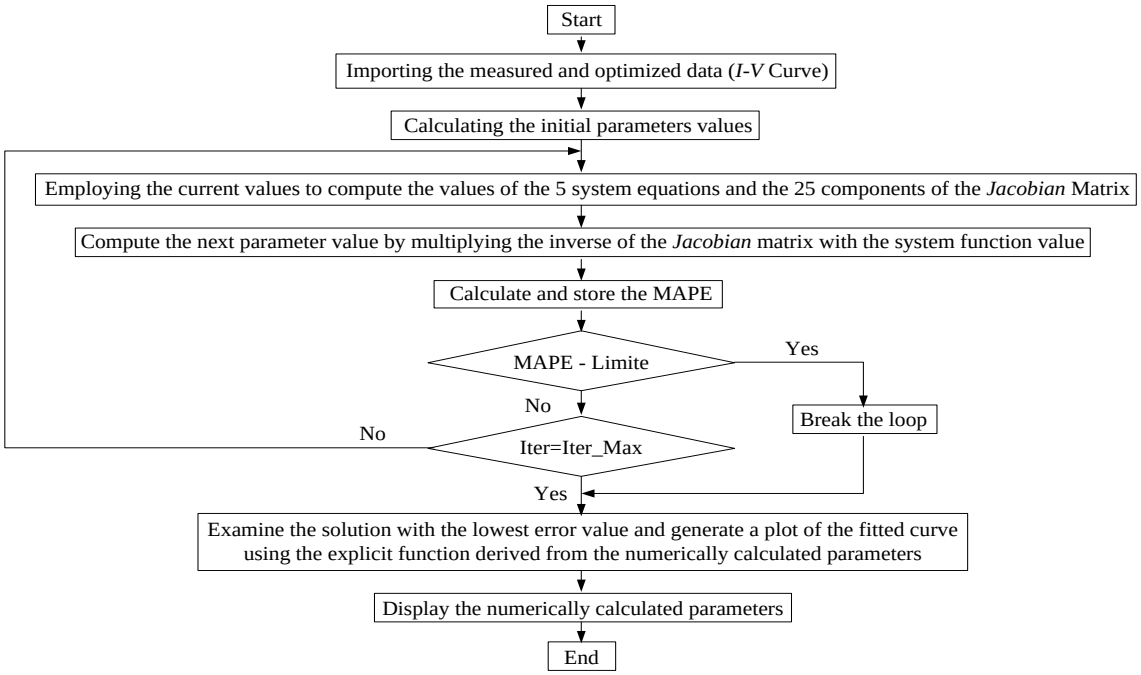

Figure 2. *Flowchart of the IRF algorithm*

For each iteration, the MAPE value is recorded together with the corresponding extracted five parameters. Upon reaching the maximum number of iterations, the stored errors are compared, and the solution with

the lowest value is chosen as the best solution. Compared to the traditional method of comparing the sum of squared errors to a specific threshold, this approach considerably improves the solution and enhances the fitting process. The main reason for this improvement is that the evaluation of the five equations generates results with differing magnitudes, causing the lowest error value (the squared sum of their solutions) to not always reflect the best fit accurately.This is because the equation with the highest value holds the most substantial influence on the overall summed error. Moreover, our suggested approach provides the flexibility to choose the desired level of accuracy, thereby reducing computational expenses. This is accomplished by comparing the computed MAPE after each iteration with a predefined threshold. When the MAPE value falls below the acceptable threshold, the iteration process concludes, and the five parameters are deemed acceptable. If the specified maximum number of iterations is not reached, the iteration will continue, as depicted in Figure 2, which illustrates the flowchart of the proposed method.

4. RESULTS AND DISCUSSION

The calculation of the five parameters for the proposed model in this study is based on the manufacturer's datasheet information for three PV modules: *Mono-Crystalline SM55*, *Multi-Crystalline MSX60*, and *Thin Film ST40*. The outcomes of these calculations are summarized in Table 1. To guarantee the reliability of our comparisons, we programmed and implemented the Heuristic iterative algorithm [25], Derivative-assisted deterministic method [26], Derivative method, and mountain-climbing algorithm [27], Honey badger algorithm [28], and Flower pollination [29] based on data acquired from their respective original authors. Regarding the computational setup, simulations and experiments were conducted on a computer equipped with an M3 8-core CPU, 10-core GPU, 512 GB storage, and 8 GB unified memory.

Table 1. *Performance analysis of various solar modules at varied irradiance and temperature levels*

PV modules	G (W/m^2)	T (°C)	Iteration	I_{ph} (A)	I_0 (A)	R_{sh} (Ω)	R_s (Ω)	n	MAPE(%)
Mono-Crystalline SM55	182	23	323	0.0431	$2.06.10^{-4}$	387.14	2.16	1.85	0.007635
	327	24	294	0.0558	$2.39.10^{-4}$	342.71	1.92	1.79	0.006922
	510	25	288	0.0663	$2.61.10^{-4}$	313.65	1.63	1.66	0.005334
	731	28	301	0.0781	$2.86.10^{-4}$	281.58	1.40	1.58	0.005019
	907	29	254	0.0892	$3.11.10^{-4}$	249.91	1.22	1.51	0.004917
	1033	29	276	0.1034	$3.43.10^{-4}$	227.03	1.05	1.47	0.004621
Multi-Crystalline MSX60	132	22	385	0.0922	$1.32.10^{-4}$	811.24	9.38	1.77	0.008020
	371	24	343	0.1134	$1.89.10^{-4}$	763.33	9.02	1.70	0.007948
	526	24	311	0.1356	$2.07.10^{-4}$	701.87	8.83	1.65	0.007314
	714	27	321	0.1562	$2.80.10^{-4}$	670.84	8.49	1.61	0.007241
	922	28	347	0.1688	$3.01.10^{-4}$	612.57	8.19	1.58	0.007192
	1094	28	355	0.1712	$3.24.10^{-4}$	593.38	7.97	1.54	0.007166
Thin Film ST40	193	24	465	0.0724	$1.35.10^{-4}$	512.22	4.25	1.80	0.007954
	312	26	428	0.0833	$1.88.10^{-4}$	488.01	4.00	1.72	0.007805
	531	27	389	0.0964	$2.37.10^{-4}$	446.96	3.76	1.64	0.007712
	702	29	397	0.1092	$2.89.10^{-4}$	419.27	3.49	1.59	0.007639
	913	31	402	0.1216	$3.32.10^{-4}$	390.06	3.20	1.55	0.007487
	1122	32	384	0.1299	$3.75.10^{-4}$	371.14	3.04	1.51	0.007306

Table 1 displays the estimated results for the 5 parameters and performance monitoring parameters of the three PV modules. These parameters were derived from *I-V* curves measured under varying insolation and temperature conditions. In order to highlight the influence of irradiance, particularly on the photo-generated current, distinct curves measured at the same temperature are chosen for the *Mono-Crystalline SM55*. The validity of the proposed method is confirmed through the utilization of *I-V* curves measured on a sunny day for the *Multi-Crystalline MSX60*. Furthermore, the validation process involves considering another environmental variation, which is characterized by a cloudy day, employing the *Thin Film ST40*. Consequently, this process includes not just controlled laboratory or sunny day settings but also conditions involving cloudy days.

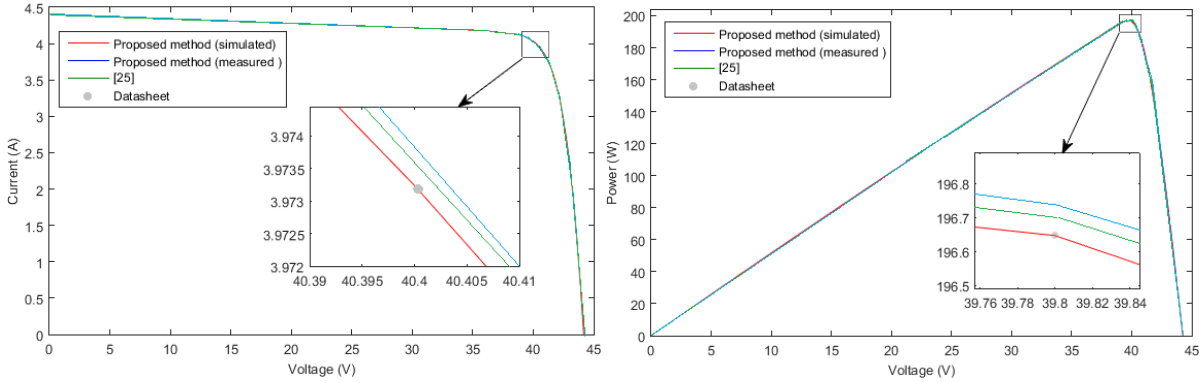

(a) (b)

Figure 3. *Simulated and measured (a) I-V and (b) P-V curves of the proposed method compared with reference [25] for the SM55 module at STC*

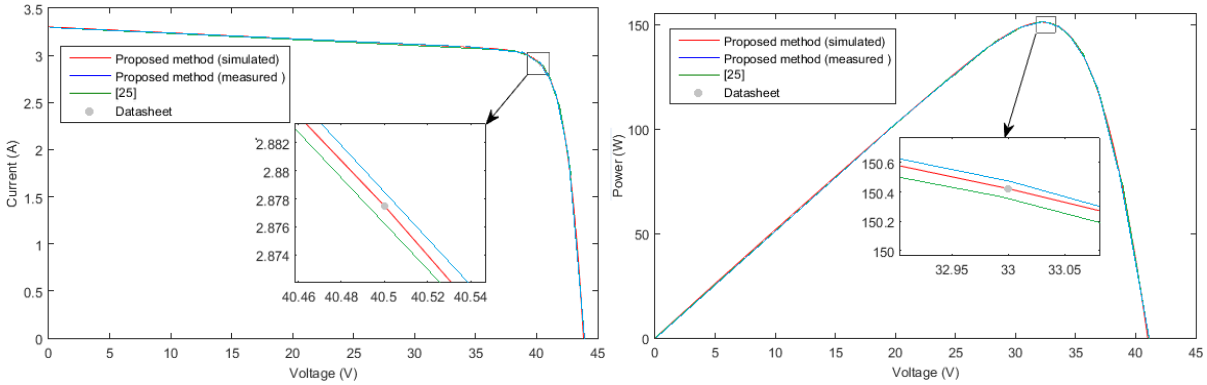

(a) (b)

Figure 4. *Simulated and measured (a) I-V and (b) P-V curves of the proposed method compared with reference [25] for the MSX-60 module at STC*

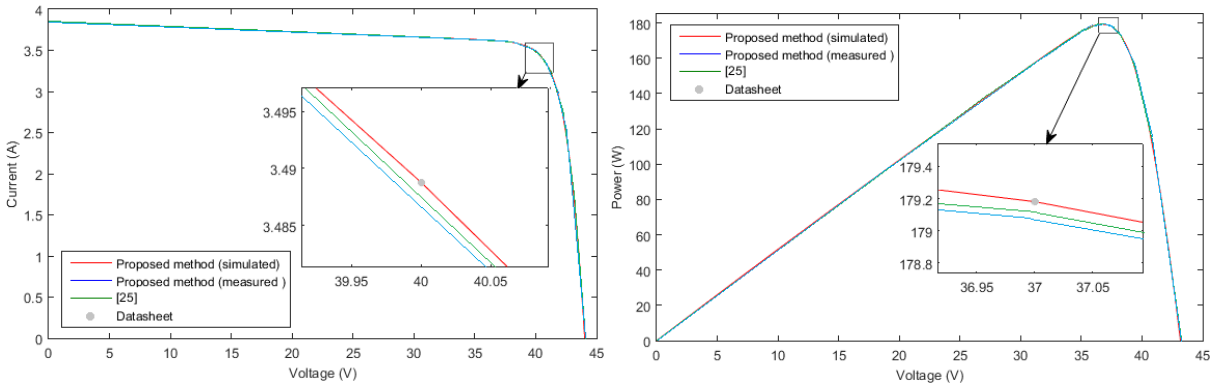

(a) (b)

Figure 5. *Simulated and measured (a) I-V and (b) P-V curves of the proposed method compared with reference [25] for the ST40 module at STC*

Figures 3, 4, and 5 display the *I-V* curves and *P-V* curves of the *MSX60, SM55 and ST40 modules*. Based on the results depicted in these figures, a strong correlation is observed between the theoretical curves obtained through simulation and the experimental data, indicating good agreement between the two. However, slight deviations can be observed, particularly around the V_{oc}, particularly under low irradiation conditions. These deviations can be attributed to certain assumptions made in the proposed parameter extraction technique. Specifically, in our proposed method, parameters like I_0 and n are assumed to be

insensitive to variations in irradiance. In other words, it is assumed that the values of these parameters remain the same under different irradiance levels as they are at standard test conditions. Another possible reason for the deviations could be the relationship between irradiance and V_{oc}.

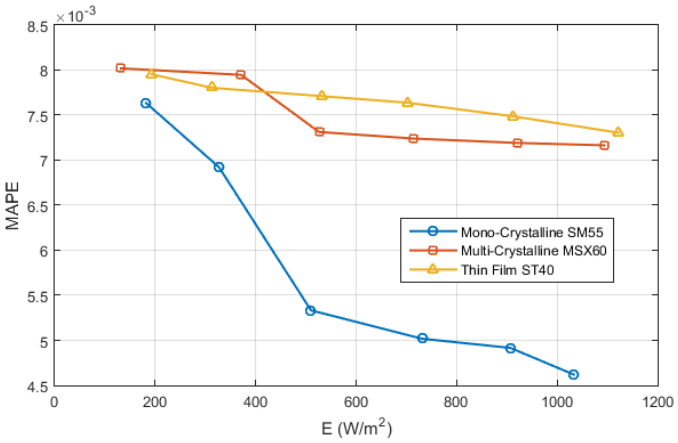

Figure 6. *MAPE as a function of irradiation for different PV modules*

Figure 6 illustrates the performance of different PV modules under varying irradiance levels. The curve depicted by circles represents the *SM55* PV module. It is evident that the MAPE gradually decreases as the irradiance increases. At low irradiance, the MAPE is higher, indicating increased uncertainty in the model's predictions compared to the actual values. Conversely, as the irradiance increases, the MAPE decreases, indicating improved module performance under higher sunlight intensity. The curve depicted by squares corresponds to the *MSX60* PV module. Similarly, the MAPE decreases with higher irradiance. However, in comparison to *SM55*, the MAPE is generally higher at all irradiance levels, indicating greater uncertainty in predictions for this particular module type. The curve depicted by triangles corresponds to the *ST40* PV module. The trend for this module shows a decrease in MAPE as irradiance increases, similar to the other modules. Notably, the MAPE for *ST40* is generally lower than that of the other two types, signifying better performance and more accurate predictions, especially at low irradiance levels.

Figure 7 shows the performance characteristics of different PV modules with varying irradiance. For all three types of modules (*SM55* in red, *MSX60* in green, and *ST40* in blue), we can observe, according to Figure 7(a), that the I_{ph} increases with an increase in irradiance. This is consistent as the current generated by solar panels is directly proportional to the amount of received sunlight. The curves representing the I_0 with respect to irradiance for each type of module (Figure 7(b)) show that I_0 increases with increasing irradiance. This trend is expected since I_0 is typically influenced by temperature, and an increase in irradiance leads to higher panel temperatures, thus increasing I_0. The R_{sh} slightly decreases with increasing irradiance for all types of modules (Figure 7(c)). This means that the current leakage through the shunt resistance increases as irradiance increases, which is not beneficial for solar panel performance. The curves representing the R_s as a function of irradiance (Figure 7(d)) show a tendency of R_s to decrease with higher irradiance for all three types of modules. This indicates that the series resistance effect becomes less pronounced as the irradiance increases. The curves representing the parameter n as a function of irradiance (Figure 7(e)) show that for the *SM55*, the ideality factor decreases significantly with increasing irradiance, indicating improved efficiency and reduced recombination losses at higher sunlight levels, making it highly suitable for environments with stable, high irradiance. The *MSX60* also shows a decrease in the ideality factor with increasing irradiance, though less pronounced, suggesting moderate performance improvement and versatility for various sunlight conditions. The *ST40* exhibits a slight decrease in the ideality factor, indicating stable but generally higher recombination losses, making it suitable for environments with variable sunlight, including low-light conditions. Overall, the *Mono-Crystalline SM55* is optimal for high irradiance environments, the *Multi-Crystalline MSX60* is a balanced choice for moderate conditions, and the *Thin Film ST40* is best for variable sunlight conditions. This understanding aids in selecting the appropriate PV module type to optimize solar energy efficiency based on specific irradiance conditions.

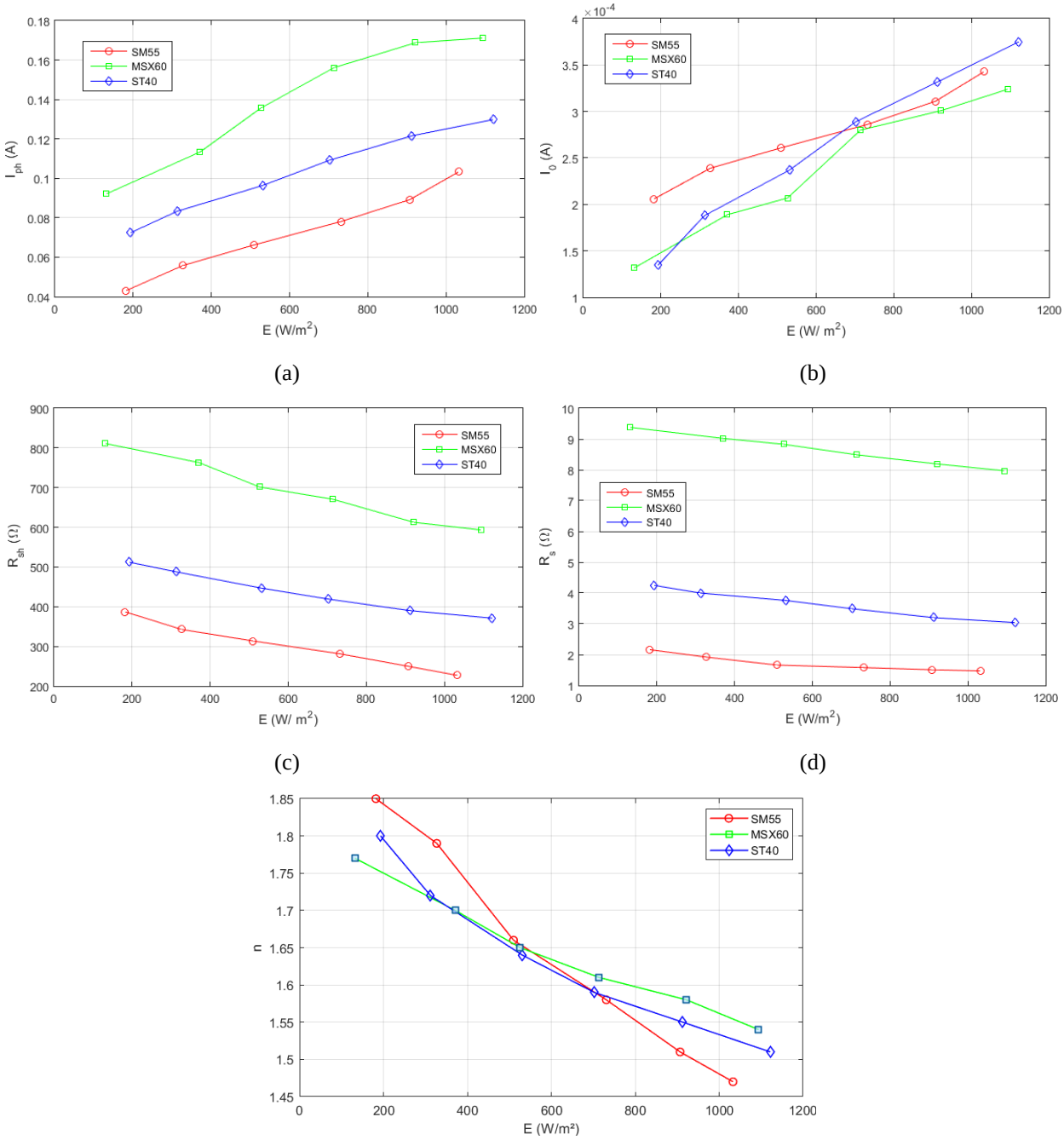

Figure 7. *Performance characteristics of different PV modules with varying irradiance: (a) I_{ph} as a function of E; (b) I_0 as a function of E; (c) R_{sh} as a function of E; (d) R_s as a function of E; (e) n as a function of E*

The Table 2 presents a comparative analysis of several algorithms applied to three types of solar cell modules: *Poly-crystalline*, *Mono-Crystalline*, and *Thin Film*. Each algorithm's performance is evaluated based on MAPE and the execution time in seconds. Our proposed algorithm showcases commendable versatility by achieving competitive MAPE values, particularly excelling in *Mono-Crystalline* modules, suggesting robust applicability across diverse solar cell types. The algorithm's moderate computational times further enhance its practical utility. *Vais* [12] introduces the Dandelion Optimization Algorithm, displaying extraordinary precision with extremely low MAPE values. However, the lack of information regarding computational times necessitates further investigation to assess its overall suitability for real-world applications, especially considering the potential trade-off between precision and computational

efficiency. *Tao's* [25] Heuristic Iterative Algorithm demonstrates consistency and competitiveness across various module types. The algorithm strikes a commendable balance between accuracy and computational efficiency, making it a strong contender for practical implementation. Further exploration could focus on understanding its sensitivity to varying input conditions and its adaptability to diverse datasets. *Xu's* [26] Derivative-assisted Deterministic Method provides moderate performance with variable MAPE values. The algorithm's computational times, although on the higher side, may still be acceptable for specific applications. Further research could delve into the algorithm's sensitivity to noise, scalability, and its robustness under different conditions. *Meng's* [27] Derivative Method with Mountain-Climbing Algorithm exhibits a favorable balance between MAPE and computational efficiency. While it shows promise, additional exploration into the algorithm's convergence behavior and its ability to handle complex, non-linear relationships would contribute to a more comprehensive understanding. *Düzenli's* [28] Honey Badger Algorithm displays noteworthy performance with low MAPE values and moderate computational times. Further validation of its robustness under diverse conditions, as well as its adaptability to various datasets, would strengthen its credibility for broader applications. *Ram's* [29] Flower Pollination Algorithm yields competitive results, albeit with variations in MAPE values. The algorithm's moderate computational times enhance its practicality, but additional research could focus on understanding its sensitivity to parameter tuning and adaptability to different problem domains. The selection of an algorithm should be informed by a careful consideration of specific application requirements, including the desired balance between accuracy and computational efficiency. Each algorithm presents unique strengths, and further research into their robustness, scalability, and adaptability to different conditions will contribute to their refinement and wider applicability.

Table 2. *Comparison of solar cell module parameter extraction algorithms: An investigation into MAPE and execution time*

Reference	Algorithm	Module type	Average MAPE	Time [s]
Douiri	Proposed method	*Poly-crystalline*	$7.314.10^{-3}$	0.64
		Thin Film	$7.639.10^{-3}$	0.80
		Mono-Crystalline	$5.019.10^{-4}$	0.72
Vais [12]	Dandelion optimisation algorithm (DOA)	*Poly-crystalline*	$4.46.10^{-16}$	-
		Thin Film	$4.93.10^{-17}$	-
		Mono-Crystalline	$6.60.10^{-16}$	-
Tao [25]	Heuristic iterative algorithm	*Poly-crystalline*	$3.4012.10^{-4}$	0.83
		Thin Film	$6.8204.10^{-4}$	0.62
		Mono-Crystalline	$5.8712.10^{-4}$	1
Xu [26]	Derivative-assisted deterministic method	*Poly-crystalline*	$1.7720.10^{-3}$	1.41
		Thin Film	$2.46.10^{-3}$	1.57
		Mono-Crystalline	$1.2267.10^{-3}$	1.28
Meng [27]	Derivative method and mountain-climbing algorithm	*Poly-crystalline*	$1.9123.10^{-3}$	0.94
		Thin Film	$1.5571.10^{-3}$	0.82
		Mono-Crystalline	$1.4302.10^{-3}$	0.81
Düzenli [28]	Honey badger algorithm	*Poly-crystalline*	$2.7429.10^{-5}$	1.09
		Thin Film	$3.5542.10^{-5}$	1.22
		Mono-Crystalline	$3.2818.10^{-5}$	1.17
Ram [29]	Flower pollination	*Poly-crystalline*	$5.87.10^{-4}$	1.4
		Thin Film	$3.65.10^{-4}$	1.89
		Mono-Crystalline	$7.27.10^{-4}$	1.2

5. CONCLUSION

This study introduces a novel iterative method for accurately extracting parameters from the PV solar cell single diode model under diverse environmental conditions. The approach comprises two main steps: an analytical step followed by an iterative process implemented numerically and experimentally to calculate the five parameters of the single diode model, namely, saturation current, serial resistance, parallel

resistance, and ideality factor. The method employs the MAPE as a criterion to determine the optimal parameter configuration for the PV solar cell. To assess the approach's performance, accuracy, and convergence, data from manufacturers for *Mono-Crystalline SM55*, *Multi-Crystalline MSX60*, and *Thin Film ST40* modules were utilized. Comparing the results of our proposed approach with those of another model from [25], it was found that our approach showed good correlation, as indicated by the *I-V* and *P-V* curves, between the estimated values and the manufacturer-provided values. The minimum values of MAPE observed were 0.00501% for *SM55*, 0.00731% for *MSX60*, and 0.00763% for *ST40* when irradiance and temperature changed. These results demonstrate that our model outperforms the [25] model in accurately extracting parameters from the single diode model.

NOMENCLATURE

PV : Photovoltaic
IRF : Iterative Root-Finding
I-V : Current-Voltage
P-V : Power-Voltage
MAPE : Mean Absolute Percentage Error
STC : Standard Test Conditions
MPP : Maximal Power Point
K : *Boltzmann* constant ($1.38.10^{-23}$ J/K)
q : Electron charge (1.6×10^{-19}C)
E_g : Energy band gap (eV)
N_c : Number of solar cells in series
I_{pv} : Output current of the cell (A)
V_{pv} : Output voltage of the cell (V)
P_{pv} : Photovoltaic power (W)
I_d : Diode current (A)
I_{ph} : Photocurrent (A)
I_{sh} : Current flowing into the shunt resistance (A)
I_0 : Diode reverse saturation current (A)
I_{rs} : Reverse saturation current (A)
R_s : Series resistance (Ω)
R_{sh} : Shunt resistance (Ω)
n : Diode ideal factor
V_t : Thermal voltage
G : Solar irradiance (W/m^2)
T : Cell temperature (K)
k_i : Temperature coefficient
V_{oc} : Open circuit voltage (V)
I_{sc} : Short circuit current (A)
$I_{ph,rf}$: Photocurrent at STC (A)
$I_{sh,rf}$: Current flowing into the shunt resistance at STC (A)
$I_{0,rf}$: Saturation current of the equivalent diode at STC (A)
$I_{rs,rf}$: Reverse saturation current of the cell at STC (A)
$R_{s,rf}$: Series resistance of the cell at STC (Ω)
$R_{sh,rf}$: Shunt resistance of the cell at STC (Ω)
G_{rf} : Solar irradiance at STC (W/m^2)
T_{rf} : Cell temperature at STC (K)
V_{ocrf} : Open circuit voltage at STC (V)
$I_{sc,rf}$: Short circuit current at STC (A)
I_{mrf} : Current at the maximum power point at STC for cell (A)
V_{mrf} : Voltage at the maximum power point at STC (V)
S^t : Vectors consisting of 5 elements at iteration t
J : *Jacobian* matrix

APPENDIX

The resulting system of non-linear equations can be formulated as follows:

$$a_1 = \frac{\partial g_1}{\partial I_{ph}} = \sum_{i=1}^{k}\left(\frac{V_i + I_i R_s}{nV_t} - 1\right) \tag{43}$$

$$b_1 = \frac{\partial g_1}{\partial I_0} = \sum_{i=1}^{k}\exp\left(\frac{V_i + I_i R_s}{nV_t} - 1\right) \tag{44}$$

$$c_1 = \frac{\partial g_1}{\partial R_{sh}} = \sum_{i=1}^{k}\left(-\frac{V_i + I_i R_s}{R_{sh}^2}\right) \tag{45}$$

$$d_1 = \frac{\partial g_1}{\partial R_s} = \sum_{i=1}^{k}\left(I_0 \frac{I_i}{nV_t}\exp\frac{V_i + I_i R_s}{nV_t} + \frac{I_i}{R_{sh}}\right) \tag{46}$$

$$e_1 = \frac{\partial g_1}{\partial n} = \sum_{i=1}^{k}\left(-I_0 \frac{V_i + I_i R_s}{n^2 V_t}\exp\frac{V_i + I_i R_s}{nV_t}\right) \tag{47}$$

$$a_2 = \frac{\partial g_2}{\partial I_{ph}} = \sum_{i=1}^{k}-\left(1 - \exp\frac{V_i + I_i R_s}{nV_t}\right) \tag{48}$$

$$b_2 = \frac{\partial g_2}{\partial I_0} = \sum_{i=1}^{k}\left(1 - \exp\frac{V_i + I_i R_s}{nV_t}\right)^2 \tag{49}$$

$$c_2 = \frac{\partial g_2}{\partial R_{sh}} = \sum_{i=1}^{k}\left(\frac{V_i + I_i R_s}{R_{sh}^2}\left(1 - \frac{V_i + I_i R_s}{nV_t}\right)\right) \tag{50}$$

$$d_2 = \frac{\partial g_2}{\partial R_s} = \sum_{i=1}^{k}\frac{I_i}{nV_t}\left(\left(I_i - I_{ph} - 2I_0 + \frac{nV_t}{R_{sh}} + \frac{V_i + I_i R_s}{R_{sh}} + 2I_0\exp\left(\frac{V_i + I_i R_s}{nV_t}\right)\right)\exp\left(\frac{V_i + I_i R_s}{nV_t}\right) - \frac{nV_t}{R_{sh}}\right) \tag{51}$$

$$e_2 = \frac{\partial g_2}{\partial n} = \sum_{i=1}^{k}\left(\left(\frac{V_i + I_i R_s}{n^2 V_t}\right)\left(I_{ph} - I_i - 2I_0\left(\frac{V_i + I_i R_s}{nV_t} - 1\right) - \frac{V_i + I_i R_s}{R_{sh}}\right)\exp\left(\frac{V_i + I_i R_s}{nV_t}\right)\right) \tag{52}$$

$$a_3 = \frac{\partial g_3}{\partial I_{ph}} = \sum_{i=1}^{k}\left(-\frac{V_i + I_i R_s}{R_{sh}^2}\right) \tag{53}$$

$$b_3 = \frac{\partial g_3}{\partial I_0} = \sum_{i=1}^{k}\left(\left(\frac{V_i + I_i R_s}{R_{sh}^2}\right)\left(\exp\left(\frac{V_i + I_i R_s}{nV_t} - 1\right)\right)\right) \tag{54}$$

$$c_3 = \frac{\partial g_3}{\partial R_{sh}} = \sum_{i=1}^{k}\left(\frac{V_i + I_i R_s}{R_{sh}^3}\left(2I_{ph} - \frac{V_i + I_i R_s}{R_{sh}} - 2I_i - 2I_0\left(\exp\left(\frac{V_i + I_i R_s}{nV_t}\right) - 1\right) - 2\frac{V_i + I_i R_s}{R_{sh}}\right)\right) \tag{55}$$

$$d_3 = \frac{\partial g_3}{\partial R_s} = \sum_{i=1}^{k}\frac{I_i}{R_{sh}^2}\left(I_0 \frac{V_i + I_i R_s}{nV_t}\exp\left(\frac{V_i + I_i R_s}{nV_t}\right) + 2\frac{V_i + I_i R_s}{R_{sh}} + I_i - I_{ph} + I_0\left(\exp\left(\frac{V_i + I_i R_s}{nV_t}\right) - 1\right)\right) \tag{56}$$

$$e_3 = \frac{\partial g_3}{\partial n} = \sum_{i=1}^{k}\left(\left(\frac{V_i + I_i R_s}{R_{sh}^2}\right)\left(-\frac{V_i + I_i R_s}{n^2 V_t}\right)\left(I_0\exp\left(\frac{V_i + I_i R_s}{nV_t}\right)\right)\right) \tag{57}$$

$$a_4 = \frac{\partial g_4}{\partial I_{ph}} = \sum_{i=1}^{k}\left(-\frac{I_i}{R_{sh}} - \frac{I_i I_0}{nV_t}\exp\left(\frac{V_i + I_i R_s}{nV_t}\right)\right) \tag{58}$$

$$b_4 = \frac{\partial g_4}{\partial I_0} = \sum_{i=1}^{k}\frac{I_i}{nV_t}\exp\left(\frac{V_i + I_i R_s}{nV_t}\right)\left(2I_0\left(\exp\left(\frac{V_i + I_i R_s}{nV_t}\right) - 1\right) + I_i - I_{ph} + \frac{V_i + I_i R_s}{R_{sh}} + \frac{I_i}{R_{sh}}\left(\exp\frac{V_i + I_i R_s}{nV_t} - 1\right)\right) \tag{59}$$

$$c_4 = \frac{\partial g_4}{\partial R_{sh}}$$

$$= \sum_{i=1}^{k} \frac{I_i}{R_{sh}^2}\left(-\frac{V_i + I_i R_s}{R_{sh}} - I_0 \frac{V_i + I_i R_s}{nV_t} \exp\frac{V_i + I_i R_s}{nV_t} - I_i + I_{ph} - I_0\left(\exp\left(\frac{V_i + I_i R_s}{nV_t} \right) - 1 \right) - \frac{V_i + I_i R_s}{R_{sh}} \right) \tag{60}$$

$$d_4 = \frac{\partial g_4}{\partial R_s}$$

$$= \sum_{i=1}^{k} \left(\left(\frac{I_0 I_i^2}{n^2 V_t^2} \exp\left(\frac{V_i + I_i R_s}{nV_t} \right) \right) \left(I_0 \exp\left(\frac{V_i + I_i R_s}{nV_t} \right) + \frac{2nV_t}{R_{sh}} + I_i + I_{ph} - I_0\left(\exp\left(\frac{V_i + I_i R_s}{nV_t} \right) - 1 \right) + \frac{V_i + I_i R_s}{R_{sh}} \right) + \frac{I_i^2}{R_{sh}^2} \right) \tag{61}$$

$$e_4 = \frac{\partial g_4}{\partial n} = \sum_{i=1}^{k} \left(-I_0 I_i \left(\frac{V_i + I_i R_s}{n^2 V_t} \right) \exp\left(\frac{V_i + I_i R_s}{nV_t} \right) \right)$$

$$\cdot \left(\frac{1}{R_{sh}} + \frac{I_0}{nV_t} \exp\left(\frac{V_i + I_i R_s}{nV_t} \right) + \left(\frac{1}{nV_t} + \frac{1}{V_i + I_i R_s} \right) \left(I_i - I_{ph} + I_0\left(\exp\left(\frac{V_i + I_i R_s}{nV_t} \right) - 1 \right) + \frac{V_i + I_i R_s}{nV_t} \right) \right) \tag{62}$$

$$a_5 = \frac{\partial g_5}{\partial I_{ph}} = \sum_{i=1}^{k} \left(-I_0 \left(\frac{V_i + I_i R_s}{n^2 V_t} \right) \exp\left(\frac{V_i + I_i R_s}{nV_t} \right) \right) \tag{63}$$

$$b_5 = \frac{\partial g_5}{\partial I_0}$$

$$= \sum_{i=1}^{k} \left(\frac{V_i + I_i R_s}{n^2 V_t} \exp\left(\frac{V_i + I_i R_s}{nV_t} \right) \right) \cdot \left(I_i - I_{ph} + 2I_0\left(\exp\left(\frac{V_i + I_i R_s}{nV_t} \right) - 1 \right) + \frac{V_i + I_i R_s}{nV_t} \right) \tag{64}$$

$$c_5 = \frac{\partial g_5}{\partial R_{sh}} = \sum_{i=1}^{k} \left(-I_0 \frac{\left(V_i + I_i R_s \right)^2}{n^2 R_{sh}^2 V_t} \exp\left(\frac{V_i + I_i R_s}{nV_t} \right) \right) \tag{65}$$

$$d_5 = \frac{\partial g_5}{\partial R_s} = \sum_{i=1}^{k} \frac{I_i I_0}{n^2 V_t} \exp\left(\frac{V_i + I_i R_s}{nV_t} \right) \left(\left(I_0 \frac{V_i + I_i R_s}{nV_t} \exp\left(\frac{V_i + I_i R_s}{nV_t} \right) \right) + \frac{V_i + I_i R_s}{R_{sh}} \right) + \left(\frac{V_i + I_i R_s}{R_{sh}} + 1 \right)$$

$$+ \left(I_i - I_{ph} + I_0\left(\exp\left(\frac{V_i + I_i R_s}{nV_t} \right) - 1 \right) + \frac{V_i + I_i R_s}{R_{sh}} \right) \tag{66}$$

$$e_5 = \frac{\partial g_5}{\partial n} = \sum_{i=1}^{k} \left(-\frac{I_0 \left(V_i + I_i R_s \right)^2}{n^4 V_t^2} \exp\left(\frac{V_i + I_i R_s}{nV_t} \right) \right)$$

$$\cdot \left(I_0 \exp\left(\frac{V_i + I_i R_s}{nV_t} \right) + \left(\frac{2nV_t}{V_i + I_i R_s} + 1 \right) \left(I_i - I_{ph} + I_0\left(\exp\left(\frac{V_i + I_i R_s}{nV_t} \right) - 1 \right) + \frac{V_i + I_i R_s}{R_{sh}} \right) \right) \tag{67}$$

CONFLICTS OF INTEREST

No conflict of interest was declared by the author.

REFERENCES

[1] Russo, M.A., Carvalho, D., Martins, N., Monteiro, A., "Forecasting the inevitable: A review on the impacts of climate change on renewable energy resources", Sustainable Energy Technologies and Assessments, 52: 102283, (2022). DOI: 10.1016/J.SETA.2022.102283

[2] AlHajri, M.F., El-Naggar, K.M., AlRashidi, M.R., Al-Othman, A.K., "Optimal extraction of solar cell parameters using pattern search", Renewable Energy, 44: 238-245, (2012). DOI: 10.1016/j.renene.2012.01.082

[3] Hejri, M., Mokhtari, H., Azizian, M.R., Ghandhari, M., Söder, L., "On the parameter extraction of a five-parameter double-diode model of photovoltaic cells and modules", IEEE Journal of Photovoltaics, 4(3): 915-923, 6756936, (2014). DOI: 10.1109/JPHOTOV.2014.2307161

[4] Abbassi, A., Ben Mehrez, R., Touaiti, B., Abualigah, L., Touti, E., "Parameterization of photovoltaic solar cell double-diode model based on improved arithmetic optimization algorithm", Optik, 253, 168600, (2022). DOI: 10.1016/J.IJLEO.2022.168600

[5] Tifidat, K., Maouhoub, N., Benahmida, A., Ezzahra Ait Salah, F., "An accurate approach for modeling I-V characteristics of photovoltaic generators based on the two-diode model", Energy Conversion and Management: X, 14, 100205, (2022). DOI: 10.1016/J.ECMX.2022.100205

[6] Barth, N., Jovanovic, R., Ahzi, S., Khaleel, M. A., "PV panel single and double diode models: Optimization of the parameters and temperature dependence", Solar Energy Materials and Solar Cells, 148:87-98, (2016). DOI: 10.1016/J.SOLMAT.2015.09.003

[7] Oh, C.-H., Go, S.-I., Choi, J.-H., Ahn, S.-J., Yun, S.-Y., "Voltage estimation method for power distribution networks using high-precision measurements", Energies, 13(9): 2385, 2020. DOI: 10.3390/en13092385

[8] Ye, K., Zhao, J., Zhang, Y., Liu, X., Zhang, H., "A generalized computationally efficient copula-polynomial chaos framework for probabilistic power flow considering nonlinear correlations of PV injections", International Journal of Electrical Power & Energy Systems, 136, 107727, (2022). DOI: 10.1016/J.IJEPES.2021.107727

[9] Nazir, R., Kanada, K., Syafii, Coveria, P., "Optimization active and reactive power flow for PV connected to grid system using Newton Raphson method", Energy Procedia, 68: 77-86, (2015). DOI: 10.1016/J.EGYPRO.2015.03.235

[10] Grisales-Noreña, L.F., Rosales-Muñoz, A.A., Cortés-Caicedo, B., Montoya, O.D., Andrade, F., "Optimal operation of PV sources in DC grids for improving technical, economical, and environmental conditions by using vortex search algorithm and a matrix hourly power flow", Mathematics, 11(1): 93, (2023). DOI: 10.3390/math11010093

[11] Rasheed, M., Al-Darraji, M.N., Shihab, S., Rashid, A., Rashid, T., "Solar PV Modelling and Parameter Extraction Using Iterative Algorithms", Journal of Physics: Conference Series, 1963(1): 012059, (2021). DOI: 10.1088/1742-6596/1963/1/012059

[12] Vais, R.I., Sahay, K., Chiranjeevi, T., Devarapalli, R., Knypiński, Ł., "Parameter Extraction of Solar Photovoltaic Modules Using a Novel Bio-Inspired Swarm Intelligence Optimisation Algorithm",Sustainability (Switzerland), 15(10): 8407, (2023). DOI: 10.3390/su15108407

[13] Belabbes, F., Cotfas, D.T., Cotfas, P.A., Medles, M., "Using the snake optimization metaheuristic algorithms to extract the photovoltaic cells parameters", Energy Conversion and Management, 292, 117373, (2023). DOI: 10.1016/j.enconman.2023.117373

[14] Gu, Z., Xiong, G., Fu, X., Mohamed, A. W., Al-Betar, M. A., Chen, H., Chen, J., "Extracting accurate parameters of photovoltaic cell models via elite learning adaptive differential evolution", Energy Conversion and Management, 285, 116994, (2023). DOI: 10.1016/j.enconman.2023.116994

[15] Abdel-Basset, M., El-Shahat, D., Sallam, K.M., Munasinghe, K., "Parameter extraction of photovoltaic models using a memory-based improved gorilla troops optimizer", Energy Conversion and Management, 252, 115134, (2022). DOI: 10.1016/j.enconman.2021.115134

[16] Tan, W.-H., Mohamad-Saleh, J., "Modified normative fish swarm algorithm for optimizing power extraction in photovoltaic systems", Evolutionary Intelligence, 16(4): 1135-1154, (2023). DOI: 10.1007/s12065-022-00724-z

[17] He, P., Xi, X., Li, S., Qin, W., Xing, C., "Radial basis function based meta-heuristic algorithms for parameter extraction of photovoltaic cell", Processes, 11(6): 1606, (2023). DOI: 10.3390/pr11061606

[18] Ayyarao, T.S.L.V., Kishore, G.I., "Parameter estimation of solar PV models with artificial humming bird optimization algorithm using various objective functions", Soft Computing, (2023). DOI: 10.1007/s00500-023-08630-x

[19] Mohammed Ridha, H., Hizam, H., Mirjalili, S., Othman, M. L., Ya'acob, M. E., Ahmadipour, M., "Novel parameter extraction for Single, Double, and three diodes photovoltaic models based on robust adaptive arithmetic optimization algorithm and adaptive damping method of Berndt-Hall-Hall-Hausman", Solar Energy, 243: 35–61, (2022). DOI: 10.1016/J.SOLENER.2022.07.029

[20] Díaz, S.R., "A generalized theoretical approach for solar cells fill factors by using Shockley diode model and Lambert W-function: A review comparing theory and experimental data", Physica B: Condensed Matter, 624, 413427, (2022). DOI: 10.1016/J.PHYSB.2021.413427

[21] Asbayou, A., Soussi, A., Isknan, I., Aamoume, A., El Fanaoui, A., Ihlal, A., Bouhouch, L., "Method using simple RLC circuit for electrical characterization of PV panels", Materials Today: Proceedings, 58: 1033-1038, (2022). DOI: 10.1016/J.MATPR.2022.01.034

[22] Kalliojärvi-Viljakainen, H., Lappalainen, K., Valkealahti, S., "A novel procedure for identifying the parameters of the single-diode model and the operating conditions of a photovoltaic module from measured current–voltage curves", Energy Reports, 8: 4633–4640, (2022). DOI: 10.1016/J.EGYR.2022.03.141

[23] Paci, B., Generosi, A., Rossi Albertini, V., Perfetti, P., de Bettignies, R., Sentein, C., "Photo-degradation and stabilization effects in operating organic photovoltaic devices by joint photo-current and morphological monitoring", Solar Energy Materials and Solar Cells, 92(7): 799–804, (2008). DOI: 10.1016/J.SOLMAT.2008.02.019

[24] Ridha, H. M., Hizam, H., Mirjalili, S., Othman, M. L., Ya'acob, M. E., Ahmadipour, M., "Parameter extraction of single, double, and three diodes photovoltaic model based on guaranteed convergence arithmetic optimization algorithm and modified third order Newton Raphson methods", Renewable and Sustainable Energy Reviews, 162, 112436, (2022). DOI: 10.1016/J.RSER.2022.112436

[25] Tao, Y., Bai, J., Pachauri, R.K., Sharma, A., "Parameter extraction of photovoltaic modules using a heuristic iterative algorithm", Energy Conversion and Management, 224, 113386, (2020). DOI: 10.1016/j.enconman.2020.113386

[26] Xu, J., Zhou, C., Li, W., "Photovoltaic single diode model parameter extraction by dI/dV-assisted deterministic method", Solar Energy, 251: 30-38, (2023). DOI: 10.1016/j.solener.2023.01.009

[27] Meng, Z., Zhao, Y., Tang, S., Sun, Y., "An efficient datasheet-based parameters extraction method for two-diode photovoltaic cell and cells model", Renewable Energy, 153: 1174-1182, (2020). DOI: 10.1016/j.renene.2020.02.084

[28] Düzenli, T., Kutlu Onay, F., Aydemir, S.B., "Improved honey badger algorithms for parameter extraction in photovoltaic models", Optik, 268, 169731, (2022). DOI: 10.1016/j.ijleo.2022.169731

[29] Ram, J.P., Babu, T.S., Dragicevic, T., Rajasekar, N., "A new hybrid bee pollinator flower pollination algorithm for solar PV parameter estimation", Energy Conversion and Management, 135: 463-476, (2017). DOI: 10.1016/j.enconman.2016.12.082